Propagation of Dirac waves through various temporal interfaces, slabs, and crystals

Seulong Kim

Research Institute of Basic Sciences, Ajou University, Suwon 16499, Korea

Kihong Kim ⊙*

Department of Physics, Ajou University, Suwon 16499, Korea
and School of Physics, Korea Institute for Advanced Study, Seoul 02455, Korea

We investigate the influence of the temporal variations of various medium parameters on the propagation of Dirac-type waves in materials where the quasiparticles are described by a generalized version of the pseudospin-1/2 Dirac equation. Our considerations also include the propagation of electromagnetic waves in metamaterials with the Dirac-type dispersion. We focus on the variations of the scalar and vector potentials, mass, Fermi velocity, and tilt velocity describing the Dirac cone tilt. We derive the scattering coefficients associated with the temporal interfaces and slabs analytically and find that the temporal scattering is caused by the changes of the mass, Fermi velocity, and vector potential, but does not arise from the changes of the scalar potential and tilt velocity. We also explore the conditions under which the temporal Brewster effect and total interband transition occur and calculate the change in total wave energy. We examine bilayer Dirac temporal crystals where parameters switch between two different sets of values periodically and prove that these systems do not have momentum gaps. Finally, we assess the potential for observing these temporal scattering effects in experiments.

I. INTRODUCTION

The propagation of waves in time-varying media where the medium parameters vary as a function of time is an old topic that has been studied extensively in many branches of physics and engineering [1–4]. Since quantum particles can be described by wave equations such as the Schrödinger, Dirac, and Klein-Gordon equations in many physical situations, this topic is also relevant for the study of quantum materials as well as of the propagation of classical waves. Recently, there has been a strong renewed interest in the propagation of electromagnetic waves in time-varying dielectric media, where the temporal variation of the dielectric permittivity or other parameters causes various temporal scattering effects such as the temporal reflection and refraction [5–12]. The temporal reflection refers to the appearance of backward propagating waves due to a temporal variation of the medium parameters. Many other interesting phenomena including temporal circular birefringence, temporal aiming, and temporal Brewster angle have been proposed to arise in general anisotropic and bianisotropic media [13–17]. In the presence of periodic temporal variations, it has been long known that there appear momentum gaps (or k gaps), which are analogous to the

frequency gaps appearing in spatially periodic photonic crystals [18–22]. Wave propagation in such photonic temporal crystals has been studied in the framework of the Floquet analysis [23].

In contrast to the extensive research on the photonics of time-varying media, there have been far fewer studies on similar problems for quantum wave equations. In the case of the Schrödinger equation, the temporal scattering does not occur because it is a first-order differential equation in time. However, the temporal scattering does occur in the systems governed by relativistic wave equations such as the Dirac and Klein-Gordon equations. For the Dirac equation in two dimensions, the temporal scattering effect due to the variation of the mass term has been studied recently in the context of quantum time mirrors [24–26]. In this paper, we study the propagation of waves governed by a generalized form of the pseudospin-1/2 Dirac equation in the presence of various kinds of time-varying perturbations. More specifically, we consider the temporal variations of the scalar and vector potentials, Fermi velocity, tilt velocity describing the magnitude and the direction of the Dirac cone tilt, and mass describing the band gap between the upper and lower Dirac cones. For the simplest configurations such as temporal interfaces and slabs, we derive the analytical expressions of the temporal scattering coefficients and prove that the variations of the vector potential, Fermi velocity, and mass cause the temporal scattering effects, whereas those of the scalar potential and tilt velocity do not. We also derive analytically the explicit conditions for the temporal equivalents of the total transmission and the total interband transition. The temporal total transmission may also be called temporal Brewster effect [17]. In addition, we derive

*khkim@ajou.ac.kr

the expressions for the change of the total wave energy for temporal interfaces and slabs. In the case of bilayer temporal crystals where the medium parameters alternate between two different values periodically in time, we prove that the momentum gaps never appear in the systems satisfying the pseudospin-1/2 Dirac equation. This is in a sharp contrast to the case of electromagnetic waves and other classical waves.

There exist many two- and three-dimensional materials where the quasiparticles satisfy the generalized pseudospin-1/2 Dirac equation [27–30]. In such materials, temporal variations of the vector potential, Fermi velocity, and mass can be readily realized experimentally and the consequences of the temporal scattering will be manifested in various transport properties. On the other hand, it is possible to fabricate electromagnetic and elastic metamaterials mimicking the Dirac materials where the dispersion relations are of the Dirac type [31–35]. The phenomena investigated in the present study can also be tested in experiments involving such metamaterials.

The rest of this paper is organized as follows. In Sec. II, we introduce a generalized version of the pseudospin-1/2 Dirac equation in two dimensions. In Sec. III, we derive the temporal scattering coefficients for temporal interfaces and the conditions for the temporal Brewster effect and total interband transition analytically. We also derive the expressions for the change of the total wave energy. Similar calculations are performed for temporal slabs in Sec. IV. In Sec. V, we derive the dispersion relations for general bilayer Dirac temporal crystals and prove that there never appears a momentum gap in such systems. Finally, we give a brief discussion of the experimental feasibility of the effects considered in this work and conclude the paper in Sec. VI.

II. WAVE EQUATION

We consider a generalized form of the effective Hamiltonian for massive pseudospin-1/2 Dirac particles moving in the two-dimensional (2D) xy plane given by

$$\mathcal{H} = v_x \sigma_x \pi_x + v_y \sigma_y \pi_y + (v_{tx}\pi_x + v_{ty}\pi_y)I + UI + M\sigma_z$$

$$= \begin{pmatrix} v_{tx}\pi_x + v_{ty}\pi_y + U + M & v_x\pi_x - iv_y\pi_y \\ v_x\pi_x + iv_y\pi_y & v_{tx}\pi_x + v_{ty}\pi_y + U - M \end{pmatrix},$$

(1)

where

$$\pi_x = \hbar k_x + eA_x, \quad \pi_y = \hbar k_y + eA_y. \quad (2)$$

The parameters v_x and v_y are the anisotropic Fermi velocity components and v_{tx} and v_{ty} are the x and y components of the tilt velocity describing the direction and the magnitude of the Dirac cone tilt in the momentum space [36,37]. U is the scalar potential and A_x and A_y are the x and y components of the vector potential. M is the mass energy describing the energy gap between the upper and lower Dirac cones and e is the electron charge. k_x and k_y are the components of the wave vector and σ_x, σ_y, and σ_z are the Pauli matrices. I is the 2×2 unity matrix.

In this paper, we consider the situation where one or several of the parameters U, A_x, A_y, v_x, v_y, v_{tx}, v_{ty}, and M are functions of time, while being uniform in the entire space. Then the wave-vector components k_x and k_y are constants of the motion.

The time-dependent Dirac equation in two dimensions for the two-component vector wave function Ψ [= $(\psi_1, \psi_2)^T$] is

$$i\hbar \frac{d\Psi}{dt} = \mathcal{H}\Psi. \quad (3)$$

If all the parameters are constants independent of time, then we can easily solve this equation by assuming that the wave function depends on time as $e^{-i\omega t}$. The dispersion relation that follows from this takes the form

$$\omega = \mathbf{v}_t \cdot \mathbf{q} + \frac{U}{\hbar} \pm \Omega, \quad (4)$$

where

$$\Omega = \sqrt{\mu^2 + |v|^2}, \quad \mu = \frac{M}{\hbar}, \quad v = v_x q_x - iv_y q_y,$$

$$\mathbf{q} = \mathbf{k} + \frac{e\mathbf{A}}{\hbar}. \quad (5)$$

$\mathbf{v}_t$, $\mathbf{q}$, $\mathbf{k}$, and $\mathbf{A}$ are 2D vectors with the x and y components. The two solutions with the plus and minus signs represent, respectively, the particlelike and holelike bands corresponding to the upper and lower Dirac cones. The group velocities for the two bands, which we call p and h bands, respectively, are given by

$$\mathbf{v}_g = (v_{gx}, v_{gy})^T = \left(\frac{\partial\omega}{\partial k_x}, \frac{\partial\omega}{\partial k_y} \right)^T$$

$$= \begin{cases} \mathbf{v}_t + \frac{1}{\Omega}\left(v_x^2 q_x, v_y^2 q_y\right)^T, & p \text{ band} \\ \mathbf{v}_t - \frac{1}{\Omega}\left(v_x^2 q_x, v_y^2 q_y\right)^T, & h \text{ band.} \end{cases}$$

(6)

When the tilt velocity $\mathbf{v}_t$ or the vector potential $\mathbf{A}$ is nonzero, or when the Fermi velocity is anisotropic such that $v_x \neq v_y$, the group velocity becomes anisotropic. In the absence of the tilt, the group velocities for the p and h bands are directed precisely opposite to each other. We notice that $\mathbf{v}_g$ depends on $\mathbf{v}_t$, $\mathbf{v}$ [= $(v_x, v_y)^T$], $\mathbf{A}$, and M, but is independent of U.

In the stationary regime, the two components of the wave function, ψ_1 and ψ_2, are proportional to each other so that

$$\psi_2 = \begin{cases} \chi_p \psi_1, & p \text{ band} \\ \chi_h \psi_1, & h \text{ band,} \end{cases} \quad (7)$$

where

$$\chi_p = \frac{\Omega - \mu}{v}, \quad \chi_h = -\frac{\Omega + \mu}{v}. \quad (8)$$

The quantities χ_p and χ_h can be considered as the effective wave impedances for p- and h-band waves, respectively.

III. TEMPORAL INTERFACE

A. Temporal scattering coefficients

We assume that, at $t = t_0$, the parameters U, A_x, A_y, v_x, v_y, v_{tx}, v_{ty}, and M change from $U_1, A_{x1}, A_{y1}, v_{x1}, v_{y1}, v_{tx1}, v_{ty1}$, and M_1 to $U_2, A_{x2}, A_{y2}, v_{x2}, v_{y2}, v_{tx2}, v_{ty2}$, and M_2 abruptly. Let us first suppose that the state before the change is a p-band state. Then the wave functions before and after the temporal change

can be written as

$$
\Psi = \begin{cases} \begin{pmatrix} 1 \\ \chi_{p1} \end{pmatrix} e^{-i\omega_{p1}(t-t_0)}, & \text{if } t < t_0 \\[2ex] S_{pp} \begin{pmatrix} 1 \\ \chi_{p2} \end{pmatrix} e^{-i\omega_{p2}(t-t_0)} + S_{hp} \begin{pmatrix} 1 \\ \chi_{h2} \end{pmatrix} e^{-i\omega_{h2}(t-t_0)}, & \text{if } t \geqslant t_0, \end{cases} \tag{9}
$$

where ω_{pj}, ω_{hj}, χ_{pj}, and χ_{hj} $(j = 1, 2)$ are defined by

$$
\omega_{pj} = v_{txj}q_{xj} + v_{tyj}q_{yj} + \frac{U_j}{\hbar} + \Omega_j,
$$

$$
\omega_{hj} = v_{txj}q_{xj} + v_{tyj}q_{yj} + \frac{U_j}{\hbar} - \Omega_j,
$$

$$
\chi_{pj} = \frac{\Omega_j - \mu_j}{v_j}, \quad \chi_{hj} = -\frac{\Omega_j + \mu_j}{v_j},
$$

$$
\Omega_j = \sqrt{\mu_j{}^2 + |v_j|^2}, \quad \mu_j = \frac{M_j}{\hbar}, \quad v_j = v_{xj}q_{xj} - iv_{yj}q_{yj},
$$

$$
q_{xj} = k_x + \frac{eA_{xj}}{\hbar}, \quad q_{yj} = k_y + \frac{eA_{yj}}{\hbar}, \tag{10}
$$

$$
\Psi = \begin{cases} \begin{pmatrix} 1 \\ \chi_{h1} \end{pmatrix} e^{-i\omega_{h1}(t-t_0)}, & \text{if } t < t_0 \\[2ex] S_{hh} \begin{pmatrix} 1 \\ \chi_{h2} \end{pmatrix} e^{-i\omega_{h2}(t-t_0)} + S_{ph} \begin{pmatrix} 1 \\ \chi_{p2} \end{pmatrix} e^{-i\omega_{p2}(t-t_0)}, & \text{if } t \geqslant t_0, \end{cases} \tag{12}
$$

where the scattering coefficients S_{hh} and S_{ph} representing $h \to h$ and $h \to p$ transitions, respectively, are given by

$$
S_{hh} = \frac{\chi_{p2} - \chi_{h1}}{\chi_{p2} - \chi_{h2}} = \frac{v_2}{2\Omega_2}\left(\frac{\Omega_1 + \mu_1}{v_1} + \frac{\Omega_2 - \mu_2}{v_2}\right),
$$

$$
S_{ph} = \frac{\chi_{h1} - \chi_{h2}}{\chi_{p2} - \chi_{h2}} = \frac{v_2}{2\Omega_2}\left(-\frac{\Omega_1 + \mu_1}{v_1} + \frac{\Omega_2 + \mu_2}{v_2}\right). \tag{13}
$$

The scattering coefficients S_{pp}, S_{hp}, S_{hh}, and S_{ph} depend on Ω_j, μ_j, and v_j $(j = 1, 2)$, which in turn depend on M_j, $\mathbf{v}_j$, and $\mathbf{A}_j$, but not on U_j and v_{tj}. In other words, temporal variations of the mass, Fermi velocity, and vector potential cause temporal scattering, but those of the scalar potential and tilt velocity do not.

In Fig. 1(a), we show a schematic of the temporal scattering process through a temporal interface at $t = t_0$, where the blue and red arrows denote the group velocities of p- and h-band waves, respectively. In the absence of Dirac cone tilt, the two group velocities are directed in precisely opposite directions.

In Fig. 2, we show schematics of the temporal scattering due to sudden changes of U, $\mathbf{v}_t$, M, $\mathbf{v}$, and $\mathbf{A}$. When the scalar potential is varied, there appears neither the scattered wave nor the change of the group velocity. When the tilt velocity is varied, there appears no scattered wave, but the group velocity is changed. When the mass is varied in the absence of Dirac cone tilt, the group velocities of the scattered waves are the same as or opposite to that of the initial wave. When the Fermi velocity or the vector potential is varied, the group velocities of the scattered waves are generally not parallel or antiparallel to that of the initial wave. If the mass is zero all the time in

and S_{pp} and S_{hp} are the intraband and interband scattering coefficients representing $p \to p$ and $p \to h$ transitions, respectively. From the continuity of Ψ at the temporal interface at $t = t_0$, we obtain

$$
S_{pp} = \frac{\chi_{p1} - \chi_{h2}}{\chi_{p2} - \chi_{h2}} = \frac{v_2}{2\Omega_2}\left(\frac{\Omega_1 - \mu_1}{v_1} + \frac{\Omega_2 + \mu_2}{v_2}\right),
$$

$$
S_{hp} = \frac{\chi_{p2} - \chi_{p1}}{\chi_{p2} - \chi_{h2}} = \frac{v_2}{2\Omega_2}\left(-\frac{\Omega_1 - \mu_1}{v_1} + \frac{\Omega_2 - \mu_2}{v_2}\right). \tag{11}
$$

Similarly, when the state before the temporal change is a h-band state, the wave functions can be written as

this case, some special situations can occur as is explained in the next section.

B. Temporal Brewster effect and temporal total interband transition

Let us suppose that the relationships

$$
v_{x1}q_{x1} = v_{x1}\left(k_x + \frac{eA_{x1}}{\hbar}\right)
$$

$$
= bv_{x2}q_{x2} = bv_{x2}\left(k_x + \frac{eA_{x2}}{\hbar}\right),
$$

$$
v_{y1}q_{y1} = v_{y1}\left(k_y + \frac{eA_{y1}}{\hbar}\right)
$$

$$
= bv_{y2}q_{y2} = bv_{y2}\left(k_y + \frac{eA_{y2}}{\hbar}\right),
$$

$$
M_1 = bM_2 \tag{14}
$$

are satisfied with b a positive proportionality constant. Then it is easy to show that the wave impedances are matched such that $\chi_{p1} = \chi_{p2}$ and $\chi_{h1} = \chi_{h2}$ and the interband scattering coefficients S_{hp} and S_{ph} vanish, while the intraband scattering coefficients (or transmission coefficients) S_{pp} and S_{hh} become unity. This phenomenon is an equivalent of the temporal Brewster effect (or temporal total transmission) for electromagnetic waves in time-varying dielectric media [17]. Similarly, when the relationships, Eq. (14), are satisfied with $b < 0$, the wave impedances are cross-matched such
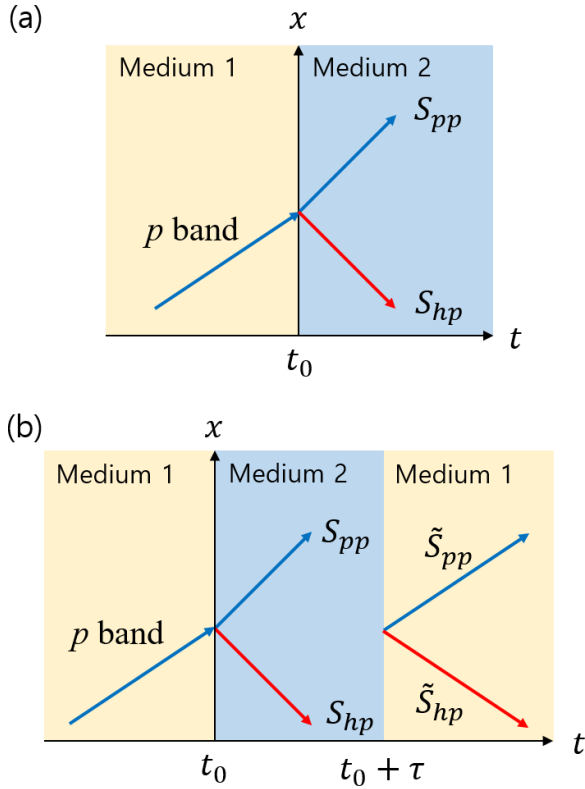
(a)

(b)

FIG. 1. Schematics of the temporal scattering processes of waves satisfying the generalized Dirac equation through (a) a temporal interface at $t = t_0$ and (b) a temporal slab of interval τ, when a p-band wave propagates initially in a uniform medium. The blue and red arrows denote the group velocities of p- and h-band waves, respectively. In the absence of Dirac cone tilt, the two group velocities are directed in precisely opposite directions. S_{pp} and S_{hp} denote the intraband and interband scattering coefficients representing $p \rightarrow p$ and $p \rightarrow h$ transitions at the interface at $t = t_0$, respectively. In (b), $\tilde{S}_{pp}$ and $\tilde{S}_{hp}$ denote the scattering coefficients for the temporal slab of interval τ.

(a) Medium 1 ($t < t_0$)

Medium 2 ($t > t_0$)

(b) $U_1 \rightarrow U_2$

(c) $\boldsymbol{v}_{t1} \rightarrow \boldsymbol{v}_{t2}$

(d) $M_1 \rightarrow M_2$

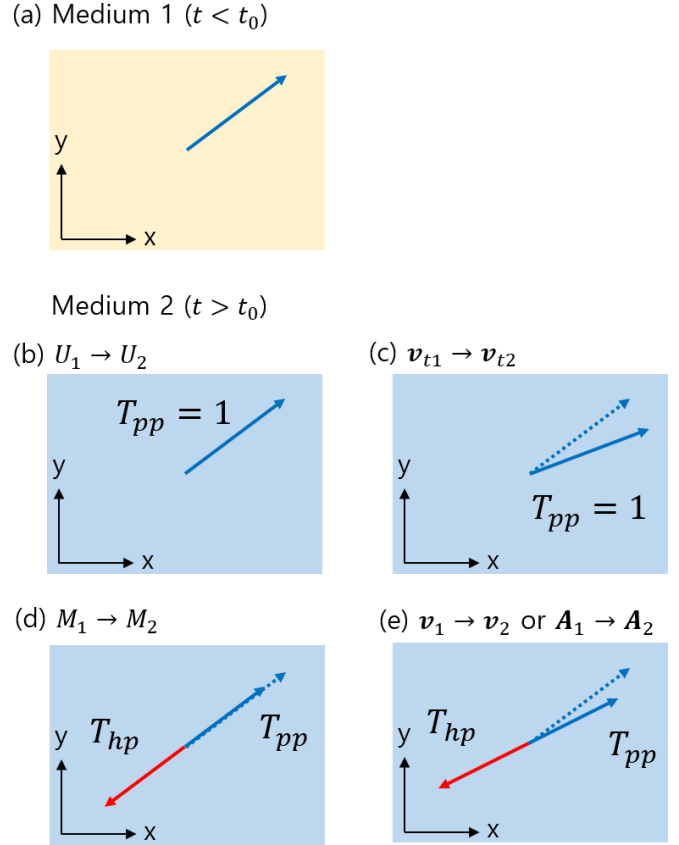(e) $\boldsymbol{v}_1 \rightarrow \boldsymbol{v}_2$ or $\boldsymbol{A}_1 \rightarrow \boldsymbol{A}_2$

FIG. 2. Schematics of the temporal scattering of (a) a p-band wave propagating in a uniform medium due to sudden changes of (b) the scalar potential, (c) tilt velocity, (d) mass, (e) Fermi velocity or vector potential. The blue and red arrows denote the group velocities of p- and h-band waves, respectively. The dotted and straight arrows in (b)–(e) represent the initial and scattered waves, respectively. In (b), there is neither the scattered h-band wave nor the change of the group velocity. In (c), there is no scattered h-band wave, but the group velocity is changed. In (d), in the absence of Dirac cone tilt, the group velocities of the scattered waves are the same as or opposite to that of the initial wave. In (e), the group velocities of the scattered waves are generally not parallel or antiparallel to that of the initial wave.

that $\chi_{p1} = \chi_{h2}$ and $\chi_{h1} = \chi_{p2}$ and the intraband scattering coefficients S_{pp} and S_{hh} vanish, while the interband scattering coefficients S_{hp} and S_{ph} become unity. This can be called temporal total interband transition between the p and h bands.

The Fermi velocity components v_{xj} and v_{yj} are always positive and the wave-vector components k_x and k_y are constants of the motion. Therefore the sign of b can become negative and the temporal total interband transition can occur only when the time-varying vector potential is present and at the same time the mass changes its sign (unless both M_1 and M_2 are zero). We also notice that if both $\mathbf{k}$ and $\mathbf{A}$ are along either the x or the y axis before and after the temporal interface and if the mass is always zero, then either the temporal Brewster effect or the temporal total interband transition occurs regardless of how the Fermi velocity and the vector potential vary. More specifically, the temporal Brewster effect occurs if q_x (or q_y) does not change its sign, while the temporal total interband transition occurs if it does.

In the system of Dirac quasiparticles, the vector potential can be easily tuned by varying the external electric field $\mathbf{E}(t)$,

which satisfies

$$\mathbf{E}(t) = -\frac{\partial}{\partial t}\mathbf{A}(t). \tag{15}$$

For instance, the vector potential A_x can be changed suddenly by inducing a sharp spike of electric field in the x direction. If the electric field is approximated by $E_x(t) = J\delta(t - t_0)$, the change of A_x is given by $A_{x2} - A_{x1} = -J$. Due to the gauge symmetry, it is always possible to choose the initial vector potential A_{x1} to be zero. Then A_{x2} is given by $-J$.

From the equation of continuity obtained from the Dirac equation, we find that the probability density ρ ($= |\Psi|^2 = |\psi_1|^2 + |\psi_2|^2$) in a spatially uniform medium is a constant independent of time. Then it is straightforward to show that
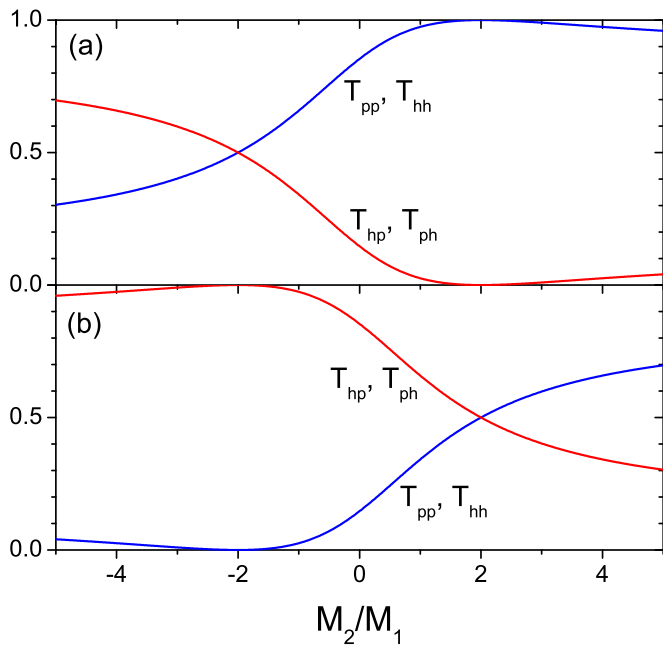
$$T_{pp} + T_{hp} = 1, \quad T_{hh} + T_{ph} = 1, \tag{16}$$

FIG. 3. Transmittances ($T_{pp} = T_{hh}$) and interband transition rates ($T_{hp} = T_{ph}$) for a temporal interface plotted versus the mass ratio M_2/M_1. The sums $T_{pp} + T_{hp}$ and $T_{hh} + T_{ph}$ are always equal to 1. The common values of the parameters are $k_y = A_{y1} = A_{y2} = 0$ and $M_1/(\hbar k_x v_{x1}) = 1$. In (a), we take $v_{x2}q_{x2} = 2v_{x1}q_{x1}$. When $M_2/M_1 = 2$, the temporal Brewster effect for which $T_{pp} = T_{hh} = 1$ arises. In (b), we take $v_{x2}q_{x2} = -2v_{x1}q_{x1}$. When $M_2/M_1 = -2$, the temporal total interband transition for which $T_{pp} = T_{hh} = 0$ arises.

where the transmittances T_{pp} and T_{hh} and the interband transition rates T_{hp} and T_{ph} are defined by

$$T_{pp} = \frac{C_{p2}}{C_{p1}}|S_{pp}|^2, \quad T_{hp} = \frac{C_{h2}}{C_{p1}}|S_{hp}|^2,$$

$$T_{hh} = \frac{C_{h2}}{C_{h1}}|S_{hh}|^2, \quad T_{ph} = \frac{C_{p2}}{C_{h1}}|S_{ph}|^2, \quad (17)$$

and

$$C_{pj} = 1 + |\chi_{pj}|^2 = 1 + \frac{(\Omega_j - \mu_j)^2}{|v_j|^2},$$

$$C_{hj} = 1 + |\chi_{hj}|^2 = 1 + \frac{(\Omega_j + \mu_j)^2}{|v_j|^2} \quad (j = 1, 2). \quad (18)$$

Furthermore, we can explicitly show that

$$T_{pp} = T_{hh} = \tfrac{1}{2}(1 + f),$$

$$T_{hp} = T_{ph} = \tfrac{1}{2}(1 - f), \quad (19)$$

where

$$f = \frac{\mu_1\mu_2 + v_{x1}v_{x2}q_{x1}q_{x2} + v_{y1}v_{y2}q_{y1}q_{y2}}{\Omega_1\Omega_2}. \quad (20)$$

When the wave impedances are matched, f is equal to 1 and T_{hp} and T_{ph} vanish, while $T_{pp} = T_{hh} = 1$. In contrast, when the impedances are cross-matched, f is equal to -1 and T_{pp} and T_{hh} vanish, while $T_{hp} = T_{ph} = 1$.

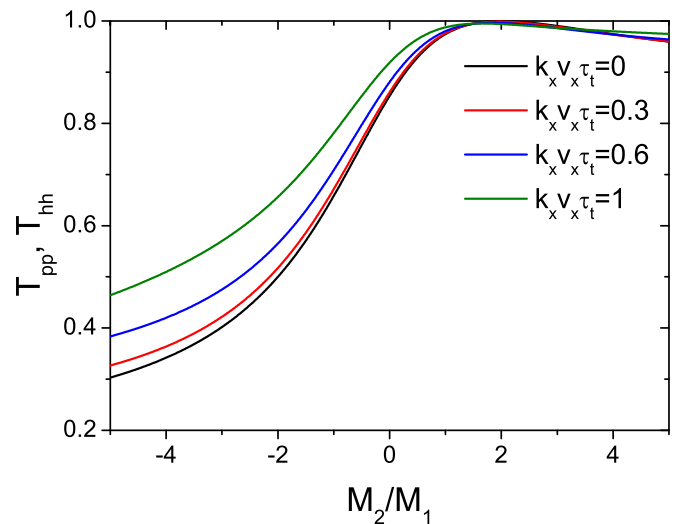In Fig. 3, we show the transmittances and the interband transition rates for a temporal interface as functions of the

FIG. 4. Transmittances ($T_{pp} = T_{hh}$) at the temporal interface corresponding to Fig. 3(a) compared to those obtained for continuous interfaces with various values of the interval τ_t. It is assumed that $k_y = A_y = 0$ and v_x is constant. Before $t = 0$, $M = M_1 = \hbar k_x v_x$ and $A_x = 0$. During the interval $0 < t < \tau_t$, M and the normalized vector potential a_x [$= eA_x/(\hbar k_x)$] change according to $M = M_1 + (M_2 - M_1)t/\tau_t$ and $a_x = (t/\tau_t)^2$, respectively. After $t = \tau_t$, they remain to be constants $M = M_2$ and $a_x = 1$. With increasing τ_t, the maximum transmittance shifts to smaller M_2/M_1 ratios, while its value remains nearly 1.

mass ratio M_2/M_1. The common values of the parameters are $k_y = A_{y1} = A_{y2} = 0$ and $M_1/(\hbar k_x v_{x1}) = 1$. In Fig. 3(a), we take $v_{x2}q_{x2} = 2v_{x1}q_{x1}$. Then the temporal Brewster effect for which $T_{pp} = T_{hh} = 1$ and $T_{hp} = T_{ph} = 0$ arises when $M_2/M_1 = 2$. In Fig. 3(b), we take $v_{x2}q_{x2} = -2v_{x1}q_{x1}$. Then the temporal total interband transition for which $T_{pp} = T_{hh} = 0$ and $T_{hp} = T_{ph} = 1$ arises when $M_2/M_1 = -2$. The variation of $v_x q_x$ can be achieved by varying v_x or A_x. For example, when $v_{x2} = v_{x1}$ and $A_{x1} = 0$, we can satisfy the conditions $v_{x2}q_{x2} = 2v_{x1}q_{x1}$ and $v_{x2}q_{x2} = -2v_{x1}q_{x1}$ if we choose a_{x2} [$\equiv eA_{x2}/(\hbar k_x)] = 1$ and -3, respectively.

Thus far, we have assumed an abrupt temporal interface characterized by instantaneous and discontinuous temporal variation. We now consider a more realistic situation in which the temporal variation takes place continuously within a finite interval. In Fig. 4, we compare the transmittance at the temporal interface corresponding to Fig. 3(a) to those obtained for continuous interfaces with various values of the interval τ_t. The numerical calculation of continuous interfaces has been conducted using the well-known invariant imbedding method [38]. We assume that $k_y = A_y = 0$ and v_x is constant. Before $t = 0$, the mass energy is $M = M_1 = \hbar k_x v_x$ and the vector potential A_x is zero. During the interval $0 < t < \tau_t$, M and the normalized vector potential a_x [$= eA_x/(\hbar k_x)$] change according to $M = M_1 + (M_2 - M_1)t/\tau_t$ and $a_x = (t/\tau_t)^2$, respectively. After $t = \tau_t$, they remain to be constants $M = M_2$ and $a_x = 1$. With increasing τ_t, the maximum transmittance shifts towards smaller M_2/M_1 ratios, while remaining close to 1. For example, when $k_x v_x \tau_t = 1$, the maximum transmittance is approximately 0.995 and occurs at $M_2/M_1 \approx 1.65$. We observe that as long as the quantity $k_x v_x \tau_t$, which is proportional

to the ratio of τ_t to the wave period, is not excessively large, the temporal Brewster effect persists in the presence of continuous temporal interfaces.

It is more pertinent to experiments to consider the propagation of wave pulses instead of plane waves. In Fig. 5, we consider the propagation of a Gaussian pulse through an abrupt temporal interface at $t = t_0$. We assume that the mass energy M and the vector potential A_x change discontinuously at $t = t_0$, while $k_y = A_y = 0$ and v_x remains constant. At $t = 0$,

$$u(x,t) = \int_{-\infty}^{\infty} D(k)\Psi(k)dk, \tag{21}$$

where

$$\Psi(k) = \begin{cases} \begin{pmatrix} 1 \\ \chi_{p1}(k) \end{pmatrix} e^{i(kx-\omega_{p1}t)}, & \text{if } t < t_0 \\ e^{i(kx-\omega_{p1}t_0)}\left[S_{pp}(k)\begin{pmatrix} 1 \\ \chi_{p2}(k) \end{pmatrix} e^{-i\omega_{p2}(t-t_0)} + S_{hp}(k)\begin{pmatrix} 1 \\ \chi_{h2}(k) \end{pmatrix} e^{-i\omega_{h2}(t-t_0)} \right], & \text{if } t \geqslant t_0, \end{cases}$$

$$D(k) = \frac{1}{\sqrt{2\pi}\sigma_k} e^{-(k-k_c)^2/2\sigma_k^2}. \tag{22}$$

The probability density plotted in Fig. 5 is obtained from

$$P(x,t) = \frac{|u(x,t)|^2}{\int_{-\infty}^{\infty} |u(x,0)|^2 dx}. \tag{23}$$

The parameter k_c denotes the central wave number and σ_k is a measure of the pulse width. In the present calculation, we set σ_k to a fixed value of $0.1k_c$. It should be noted that the frequencies ω_{p1}, ω_{p2}, and ω_{h2} are also dependent on k. In the cases shown in Figs. 5(a)–(c), M is given by $M_1 = \hbar k_c v_x$ and A_x is zero at the initial time $t = 0$. The pulse encounters a temporal interface at $t = t_0 = 5\tau_0$, where the time unit τ_0 is defined as $\tau_0 = 1/(\sigma_k v_x)$. Prior to reaching the temporal interface, the group velocity is equal to $v_x/\sqrt{2}$.

We examine four different cases that correspond to the temporal Brewster effect, partial reflection, total interband transition, and nearly total reflection. In Fig. 5(a), which represents the temporal Brewster effect, the mass transitions from M_1 to $M_2 = 2M_1$, and the normalized vector potential a_x shifts from zero to 1 at the interface. In this case, the pulse remains unaffected by the interface and continues to propagate in the same direction with an unchanged group velocity. In Fig. 5(b), where M and a_x change to $-2M_1$ and 1 at the interface, the pulse undergoes a division, propagating simultaneously in both the forward and backward directions. The p-band state pulse, moving in the $+x$ direction, advances with a group velocity of $v_x/\sqrt{2}$, while the h-band state pulse, traveling in the $-x$ direction, possesses a group velocity of $-v_x/\sqrt{2}$. In Fig. 5(c), which corresponds to the temporal total interband transition, the mass changes from M_1 to $M_2 = -2M_1$, and a_x shifts from zero to -3 at the interface. In this case, the states comprising the pulse undergo a complete transition from the p band to the h band. Nevertheless, the pulse continues to propagate in the same direction with an unchanged group velocity. This occurs because the changes in M and A_x result in the interchange of group velocities between the p and h bands. In other words, the group velocity for the h-band state after the temporal interface becomes the same as that for the p-band state before the interface. Finally, in Fig. 5(d), the mass changes from $5\hbar k_c v_x$ to $-5\hbar k_c v_x$, while the vector potential

the initial pulse consisting of p-band states is positioned at $x = 0$ and propagates towards the $+x$ direction. The Gaussian pulse is defined by

remains zero at the interface. As a result of the significant change in mass, an almost complete reflection occurs. The parameter f in Eq. (20) is equal to $-12/13$ and about 96.1% of the pulse is reflected in the opposite direction.

C. Change of the total energy

In a time-varying environment, the total energy $\mathcal{E}$ is not conserved but varies with time. We can calculate $\mathcal{E}$ using

$$\mathcal{E} = \frac{\Psi^\dagger \mathcal{H} \Psi}{|\Psi|^2}. \tag{24}$$

The wave function at an arbitrary time t can be written as

$$\Psi = c\Psi_p + d\Psi_h, \tag{25}$$

where c and d are constants and

$$\Psi_p = \begin{pmatrix} 1 \\ \chi_p \end{pmatrix} e^{-i\omega_p t}, \quad \Psi_h = \begin{pmatrix} 1 \\ \chi_h \end{pmatrix} e^{-i\omega_h t}. \tag{26}$$

Using

$$\mathcal{H}\Psi_p = \hbar\omega_p \Psi_p, \quad \mathcal{H}\Psi_h = \hbar\omega_h \Psi_h \tag{27}$$

and

$$\Psi_p^\dagger \Psi_h = \Psi_h^\dagger \Psi_p = 0, \tag{28}$$

which follows from $1 + \chi_p^* \chi_h = 1 + \chi_h^* \chi_p = 0$, we can express $\mathcal{E}$ as

$$\mathcal{E} = \frac{\hbar\omega_p |c|^2 |\Psi_p|^2 + \hbar\omega_h |d|^2 |\Psi_h|^2}{|c|^2 |\Psi_p|^2 + |d|^2 |\Psi_h|^2}. \tag{29}$$

Finally, using Eqs. (16), (17), and (18), we straightforwardly obtain the following expressions for the total wave energy after the temporal interface at $t = t_0$:

$$\mathcal{E}(t > t_0) = \begin{cases} \hbar\omega_{p2}T_{pp} + \hbar\omega_{h2}T_{hp}, & p \text{ band} \\ \hbar\omega_{h2}T_{hh} + \hbar\omega_{p2}T_{ph}, & h \text{ band}, \end{cases} \tag{30}$$
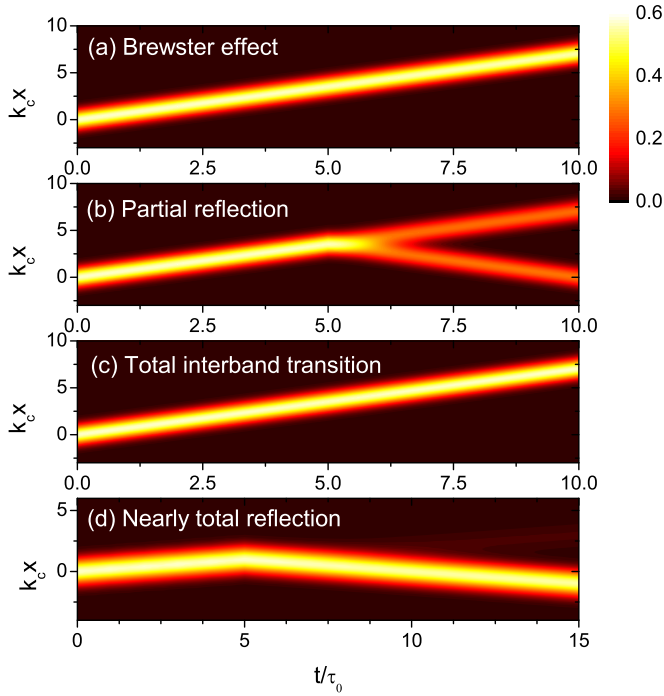
FIG. 5. Propagation of a Gaussian pulse through a sudden temporal interface occurring at $t = 5\tau_0$. It is assumed that $k_y = A_y = 0$ and v_x is constant. At $t = 0$, the pulse whose central wave number is k_c is located at $x = 0$ and propagates towards the $+x$ direction. At $t = 5\tau_0$, the mass energy M and the normalized vector potential $a_x [= eA_x/(\hbar k_c v_x)]$ change from $M_1 = \hbar k_c v_x$ and $a_{x1} = 0$ to (a) $M_2 = 2M_1$ and $a_{x2} = 1$, (b) $M_2 = -2M_1$ and $a_{x2} = 1$, (c) $M_2 = -2M_1$ and $a_{x2} = -3$. In (d), the mass changes from $5\hbar k_c v_x$ to $-5\hbar k_c v_x$, while A_x remains to be zero. The pulse width is characterized by the parameter $\sigma_k (= 0.1k_c)$ and the time unit is defined by $\tau_0 = 1/(\sigma_k v_x)$. In (b) and (d), 50% and about 96.1% of the pulse are reflected in the opposite direction, respectively.

when the states before the temporal interface are p- and h-band states, respectively. The change of $\mathcal{E}$ is given by

$$\Delta\mathcal{E} = \begin{cases} \hbar\omega_{p2}T_{pp} + \hbar\omega_{h2}T_{hp} - \hbar\omega_{p1}, & p \text{ band} \\ \hbar\omega_{h2}T_{hh} + \hbar\omega_{p2}T_{ph} - \hbar\omega_{h1}, & h \text{ band}. \end{cases} \quad (31)$$

IV. TEMPORAL SLAB

In this section, we consider a simple temporal slab of interval τ such that at $t = t_0$, the parameters change from U_1, A_{x1}, A_{y1}, v_{x1}, v_{y1}, v_{tx1}, v_{ty1}, and M_1 to U_2, A_{x2}, A_{y2}, v_{x2}, v_{y2}, v_{tx2}, v_{ty2}, and M_2, and then later at $t = t_0 + \tau$, they change back to their initial values. A schematic of the temporal scattering process through a temporal slab is shown in Fig. 1(b). Since the temporal scattering proceeds only in the $+t$ direction, we can easily obtain the scattering coefficients for the temporal slab, which we call $\tilde{S}_{pp}$, $\tilde{S}_{hp}$, $\tilde{S}_{hh}$, and $\tilde{S}_{ph}$, in terms of those for the two temporal interfaces:

$$\tilde{S}_{pp} = S_{pp}S'_{pp}e^{-i\omega_{p2}\tau} + S_{hp}S'_{ph}e^{-i\omega_{h2}\tau},$$
$$\tilde{S}_{hp} = S_{pp}S'_{hp}e^{-i\omega_{p2}\tau} + S_{hp}S'_{hh}e^{-i\omega_{h2}\tau},$$
$$\tilde{S}_{hh} = S_{hh}S'_{hh}e^{-i\omega_{h2}\tau} + S_{ph}S'_{hp}e^{-i\omega_{p2}\tau},$$
$$\tilde{S}_{ph} = S_{hh}S'_{ph}e^{-i\omega_{h2}\tau} + S_{ph}S'_{pp}e^{-i\omega_{p2}\tau}, \quad (32)$$

where the scattering coefficients for the interface at $t = t_0 + \tau$, S'_{pp}, S'_{hp}, S'_{hh}, and S'_{ph}, are obtained by exchanging Ω_1, μ_1, and v_1 with Ω_2, μ_2, and v_2, respectively, in the definitions of S_{pp}, S_{hp}, S_{hh}, and S_{ph} given by Eqs. (11) and (13). In the present case, the transmittances $\tilde{T}_{pp}$ and $\tilde{T}_{hh}$ and the interband transition rates $\tilde{T}_{hp}$ and $\tilde{T}_{ph}$ are defined by

$$\tilde{T}_{pp} = |\tilde{S}_{pp}|^2, \quad \tilde{T}_{hp} = \frac{C_{h1}}{C_{p1}}|\tilde{S}_{hp}|^2,$$

$$\tilde{T}_{hh} = |\tilde{S}_{hh}|^2, \quad \tilde{T}_{ph} = \frac{C_{p1}}{C_{h1}}|\tilde{S}_{ph}|^2. \quad (33)$$

By straightforward calculations, we obtain

$$\tilde{T}_{pp} = \tilde{T}_{hh} = 1 - (1 - f^2)\sin^2(\Omega_2\tau),$$
$$\tilde{T}_{hp} = \tilde{T}_{ph} = (1 - f^2)\sin^2(\Omega_2\tau). \quad (34)$$

The conservation laws

$$\tilde{T}_{pp} + \tilde{T}_{hp} = 1, \quad \tilde{T}_{hh} + \tilde{T}_{ph} = 1 \quad (35)$$

are easily seen to be satisfied. We note that all of $\tilde{T}_{pp}$, $\tilde{T}_{hp}$, $\tilde{T}_{hh}$, and $\tilde{T}_{ph}$ depend periodically on the interval τ with period π/Ω_2. The temporal Brewster effect occurs when $f = \pm 1$ or $\tau = n\pi/\Omega_2$ with n an arbitrary integer, whereas the temporal total interband transition occurs when $f = 0$ and $\tau = (n + 1/2)\pi/\Omega_2$ with n an arbitrary integer. In the case of $f = -1$, the temporal Brewster effect arises due to the two consecutive temporal total interband transitions at $t = 0$ and $t = \tau$. The change of the total energy when the states before the temporal slab are p- and h-band states is given by

$$\Delta\mathcal{E} = \begin{cases} -2\hbar\Omega_1(1 - f^2)\sin^2(\Omega_2\tau), & p \text{ band} \\ 2\hbar\Omega_1(1 - f^2)\sin^2(\Omega_2\tau), & h \text{ band}. \end{cases} \quad (36)$$

If we ignore the scalar potential and the tilt velocity and set $k_y = A_{y1} = A_{y2} = 0$, we can derive the explicit expressions

$$\tilde{S}_{hp} = i\frac{(\mu_1 v_2 - \mu_2 v_1)(\Omega_1 - \mu_1)}{v_1\Omega_1\Omega_2}\sin(\Omega_2\tau),$$

$$\tilde{S}_{ph} = i\frac{(\mu_1 v_2 - \mu_2 v_1)(\Omega_1 + \mu_1)}{v_1\Omega_1\Omega_2}\sin(\Omega_2\tau), \quad (37)$$

$$\tilde{T}_{hp} = \tilde{T}_{ph} = \frac{(\mu_1 v_2 - \mu_2 v_1)^2}{v_1^2\Omega_1^2\Omega_2^2}\sin^2(\Omega_2\tau).$$

In the special case where $M_1 = A_{x1} = A_{x2} = 0$ and $v_{x1} = v_{x2} = v_F$, they are simplified to

$$\tilde{S}_{hp} = \tilde{S}_{ph} = -i\frac{\mu_2}{\Omega_2}\sin(\Omega_2\tau),$$

$$\tilde{T}_{hp} = \tilde{T}_{ph} = \frac{\mu_2^2}{\Omega_2^2}\sin^2(\Omega_2\tau), \quad (38)$$

where $\Omega_2 = \sqrt{M_2^2 + (\hbar v_F k_x)^2}/\hbar$. The expression for the interband transition amplitudes $\tilde{S}_{hp}$ and $\tilde{S}_{ph}$ agrees precisely with Eq. (3) derived in Ref. [24].

In Fig. 6, we illustrate the dependencies of the interband transition rates $\tilde{T}_{hp}$ and $\tilde{T}_{ph}$ on the normalized interval $(k_x v_{x1})\tau$, mass ratio M_2/M_1, and normalized vector potential a_{x2}. In Fig. 6(a), we set $k_y = \mathbf{A}_1 = \mathbf{A}_2 = 0$, $M_1/(\hbar k_x v_{x1}) = 1$, $v_{x2}/v_{x1} = 2$, and $M_2/M_1 = 2, -2, 0$.
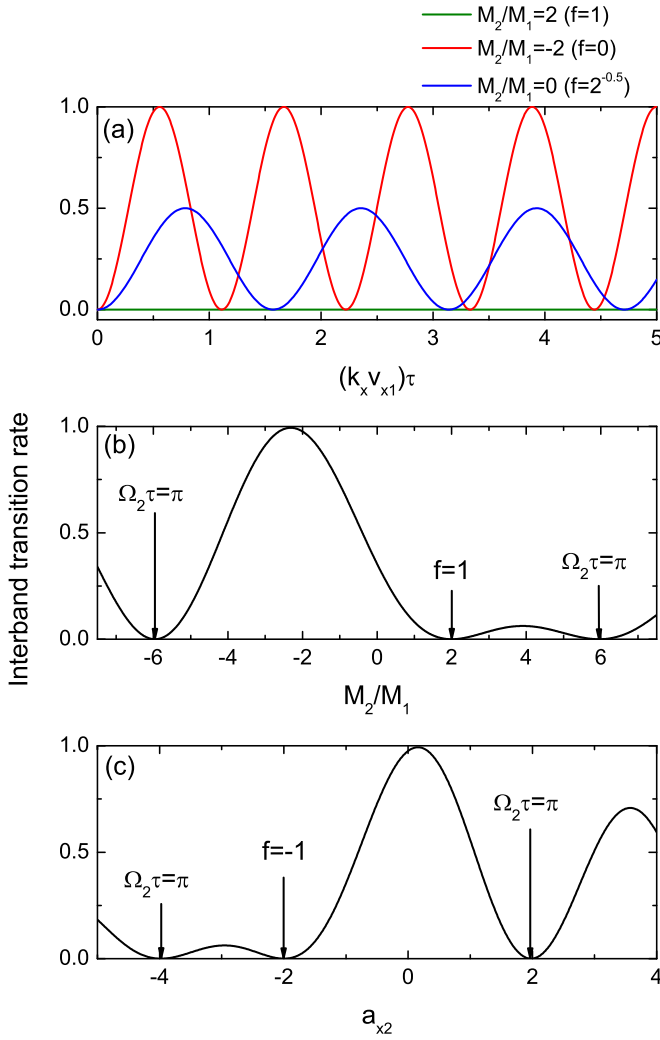
FIG. 6. Interband transition rate $\tilde{T}_{hp}$ $(= \tilde{T}_{ph})$ for a temporal slab of interval τ plotted versus (a) normalized interval $(k_x v_{x1})\tau$, (b) mass ratio M_2/M_1, and (c) normalized vector potential a_{x2} [$= eA_{x2}/(\hbar k_x)$]. In (a), we set $k_y = \mathbf{A}_1 = \mathbf{A}_2 = 0$, $M_1/(\hbar k_x v_{x1}) = 1$, $v_{x2}/v_{x1} = 2$, and $M_2/M_1 = 2, -2, 0$. For $M_2/M_1 = 2$, f is equal to 1 and $\tilde{T}_{hp} = 0$. For $M_2/M_1 = -2$, f is equal to 0 and $\tilde{T}_{hp} = \sin^2(2\sqrt{2}k_x v_{x1}\tau)$. For $M_2/M_1 = 0$, f is equal to $1/\sqrt{2}$ and $\tilde{T}_{hp} = 0.5\sin^2(2k_x v_{x1}\tau)$. In (b), we set $k_y = \mathbf{A}_1 = \mathbf{A}_2 = 0$, $M_1/(\hbar k_x v_{x1}) = 1$, $v_{x2}/v_{x1} = 2$, and $k_x v_{x1}\tau = 0.5$. The interband transition rate vanishes for either $f = 1$ corresponding to $M_2/M_1 = 2$ or $\Omega_2\tau = \pi$ corresponding to $M_2/M_1 \approx \pm 5.956$. In (c), we set $k_y = A_{x1} = A_{y1} = A_{y2} = 0$, $M_1/(\hbar k_x v_{x1}) = 1$, $M_2/M_1 = -2$, $v_{x2}/v_{x1} = 2$, and $k_x v_{x1}\tau = 0.5$. The interband transition rate vanishes for either $f = -1$ corresponding to $M_2/M_1 \approx -1.998$ or $\Omega_2\tau = \pi$ corresponding to $M_2/M_1 \approx 1.978$ and -3.978.

For $M_2/M_1 = 2$, f is equal to 1 and the interband transition rate vanishes. For $M_2/M_1 = -2$, f is equal to 0 and the interband transition rate is a periodic function given by $\tilde{T}_{hp} = \sin^2(2\sqrt{2}k_x v_{x1}\tau)$. For $M_2/M_1 = 0$, f is equal to $1/\sqrt{2}$ and $\tilde{T}_{hp} = 0.5\sin^2(2k_x v_{x1}\tau)$. In Fig. 6(b), we set $k_y = \mathbf{A}_1 = \mathbf{A}_2 = 0$, $M_1/(\hbar k_x v_{x1}) = 1$, $v_{x2}/v_{x1} = 2$, and $k_x v_{x1}\tau = 0.5$. Then the interband transition rate vanishes for either $f = 1$ corresponding to $M_2/M_1 = 2$ or $\Omega_2\tau = \pi$ corresponding to $M_2/M_1 \approx \pm 5.956$. In Fig. 6(c), we set

$k_y = A_{x1} = A_{y1} = A_{y2} = 0$, $M_1/(\hbar k_x v_{x1}) = 1$, $M_2/M_1 = -2$, $v_{x2}/v_{x1} = 2$, and $k_x v_{x1}\tau = 0.5$. Then the interband transition rate vanishes for either $f = -1$ corresponding to $M_2/M_1 \approx -1.998$ or $\Omega_2\tau = \pi$ corresponding to $M_2/M_1 \approx 1.978$ and -3.978.

V. ABSENCE OF MOMENTUM GAPS IN DIRAC TEMPORAL CRYSTALS

In the previous sections, we have shown that the temporal scattering for Dirac particles and waves can be caused by the temporal variation of the mass, Fermi velocity, and vector potential. In this section, we consider a bilayer temporal crystal where these quantities vary periodically as a function of time with period τ_p such that within one period

$$(M(t), A_x(t), A_y(t), v_x(t), v_y(t))$$
$$= \begin{cases} (M_1, A_{x1}, A_{y1}, v_{x1}, v_{y1}), & \text{if } 0 < t < t_1 \\ (M_2, A_{x2}, A_{y2}, v_{x2}, v_{y2}), & \text{if } t_1 < t < \tau_p, \end{cases} \quad (39)$$

where $\tau_p = t_1 + t_2$. We assume that the scalar potential and the tilt velocity are zero because they do not cause any temporal scattering. From the continuity of the wave function at $t = t_1$ and $t = \tau_p$ and the Floquet-Bloch theorem demanding

$$\psi(t + \tau_p) = e^{-i\Omega_p\tau_p}\psi(t), \quad (40)$$

we obtain the characteristic matrix

$$R = \begin{pmatrix} e^{-i\Omega_1 t_1} & e^{i\Omega_1 t_1} & -e^{-i\Omega_2 t_1} & -e^{i\Omega_2 t_1} \\ \chi_{p1}e^{-i\Omega_1 t_1} & \chi_{h1}e^{i\Omega_1 t_1} & -\chi_{p2}e^{-i\Omega_2 t_1} & -\chi_{h2}e^{i\Omega_2 t_1} \\ e^{-i\Omega_p\tau_p} & e^{-i\Omega_p\tau_p} & -e^{-i\Omega_2\tau_p} & -e^{i\Omega_2\tau_p} \\ \chi_{p1}e^{-i\Omega_p\tau_p} & \chi_{h1}e^{-i\Omega_p\tau_p} & -\chi_{p2}e^{-i\Omega_2\tau_p} & -\chi_{h2}e^{i\Omega_2\tau_p} \end{pmatrix}. \quad (41)$$

The frequency Ω_p is the eigenfrequency of the temporal crystal. The momentum gap would correspond to the region of the momentum (or wave vector) in which Ω_p has no real-valued solution. The dispersion relation of the temporal crystal is obtained from the condition that the determinant of R is zero and takes the simple form

$$\cos(\Omega_p\tau_p) = \cos(\Omega_1 t_1)\cos(\Omega_2 t_2) - f\sin(\Omega_1 t_1)\sin(\Omega_2 t_2)$$
$$= F\cos(\Omega_1 t_1 + \Omega_2 t_2) + G\cos(\Omega_1 t_1 - \Omega_2 t_2), \quad (42)$$

where f is defined by Eq. (20) and

$$F + G = 1, \quad F - G = f. \quad (43)$$

From this, we notice that $|\cos(\Omega_p\tau_p)|$ satisfies the inequality

$$|\cos(\Omega_p\tau_p)| \leqslant \text{Max}(1, |f|). \quad (44)$$

From the explicit form of f, we can prove that

$$(1 - f^2)(\Omega_1\Omega_2)^2 = (\mu_1 v_{x2}q_{x2} - \mu_2 v_{x1}q_{x1})^2$$
$$+ (\mu_1 v_{y2}q_{y2} - \mu_2 v_{y1}q_{y1})^2$$
$$+ (v_{x1}q_{x1}v_{y2}q_{y2} - v_{x2}q_{x2}v_{y1}q_{y1})^2 \geqslant 0. \quad (45)$$

Therefore $|f|$ is not larger than 1 and the dispersion relation always has a real solution. We conclude that there never
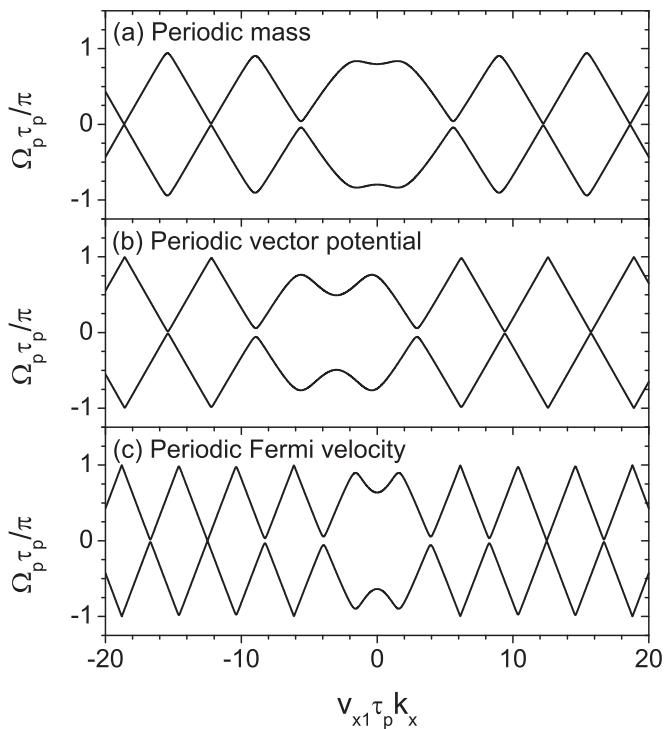
FIG. 7. Normalized frequency $\Omega_p \tau_p / \pi$ plotted versus normalized wave number $(v_{x1}\tau_p)k_x$ for bilayer Dirac temporal crystals where (a) the normalized mass $\tilde{m} = M\tau_p/\hbar$ alternates between 1 and 4 while $k_y = \mathbf{A}_1 = \mathbf{A}_2 = 0$ and $v_{x1} = v_{x2}$, (b) the normalized vector potential $v_{x1}eA_x\tau_p/\hbar$ alternates between 1 and 5 while $k_y = A_{y1} = A_{y2} = 0$, $\tilde{m}_1 = \tilde{m}_2 = 2$, and $v_{x1} = v_{x2}$, and (c) the Fermi velocity v_x alternates between v_{x1} and $2v_{x1}$ while $k_y = \mathbf{A}_1 = \mathbf{A}_2 = 0$ and $\tilde{m}_1 = \tilde{m}_2 = 2$. Only the curves in one period in the range $-1 < \Omega_p\tau_p/\pi < 1$ are displayed. These curves are repeated periodically with period 2 along the $\Omega_p\tau_p/\pi$ axis.

appears a momentum gap in bilayer Dirac temporal crystals in sharp contrast to the case of electromagnetic waves.

In Fig. 7, we show the dispersion relations for bilayer Dirac temporal crystals when the mass, vector potential, or Fermi velocity varies periodically with period τ_p. In Fig. 7(a), the normalized mass $\tilde{m} = M\tau_p/\hbar$ alternates between 1 and 4 while $k_y = \mathbf{A}_1 = \mathbf{A}_2 = 0$ and $v_{x1} = v_{x2}$. In Fig. 7(b), the normalized vector potential $v_{x1}eA_x\tau_p/\hbar$ alternates between 1 and 5 while $k_y = A_{y1} = A_{y2} = 0$, $\tilde{m}_1 = \tilde{m}_2 = 2$, and $v_{x1} = v_{x2}$. In Fig. 7(c), the Fermi velocity v_x alternates between v_{x1} and $2v_{x1}$ while $k_y = \mathbf{A}_1 = \mathbf{A}_2 = 0$ and $\tilde{m}_1 = \tilde{m}_2 = 2$. These curves are repeated periodically with period 2 along the $\Omega_p\tau_p/\pi$ axis. In all the cases, we find that there appears no momentum gap. The influence of the periodic variation is seen to be strongest in the region where $|k_x|$ is small and becomes weaker as it increases.

VI. DISCUSSION AND CONCLUSION

Let us discuss briefly the experimental feasibility of the effects explored in this paper. In 2D Dirac materials, the quantities such as the scalar and vector potentials, Fermi velocity, tilt velocity, and mass can be tuned readily by various means.

It is easy to tune the scalar potential by applying a uniform gate voltage to the whole layer [39]. A spatially uniform and time-dependent vector potential can be most easily generated by applying a uniform electric field parallel to the 2D layer [40]. It has been suggested that the mass, or the band gap between the upper and lower Dirac cones, in 2D materials such as silicene and germanene can be varied by tuning the electric field applied perpendicularly to the layer [41,42]. It has also been proposed that the Fermi velocity of the systems such as graphene nanoribbons and carbon nanotubes can be tuned by applying a uniform electric field across such materials [43]. The tilt velocity of the 8*Pmmn* borophene sheet that has tilted Dirac cones has been proposed to be tunable by applying an electric field perpendicular to the sheet [44]. There exist other systems exhibiting Dirac cones in their energy dispersion such as suitably designed photonic crystals and metamaterials and cold atoms trapped in optical lattices. It is also possible to vary the parameters of those systems temporally by various means. For example, a method to tune the effective vector potential for polaritons supported by a strained honeycomb metasurface composed of interacting dipole emitters/antennas has been proposed [45]. The variation of the parameters of cold atomic systems in optical lattices should also be possible by optical means.

The temporal scattering effects will be manifested experimentally in various physical quantities. In electronic Dirac materials, the temporal reflection of electron matter waves is expected to cause a modification in electronic currents. In quasi-one-dimensional mesoscopic systems, it has been well known that the conductance is directly proportional to the transmittance according to the Landauer formula. Therefore, through the measurement of current and conductance in the presence of temporal variations, it is feasible to experimentally investigate the effects of temporal reflection. In photonic metamaterials exhibiting Dirac-type dispersion, it should be possible to study directly the propagation of electromagnetic wave pulses similar to those considered in Fig. 5. In all of these cases, the observability can be assessed by evaluating the relative change in wave transmittance caused by temporal variations. Let us suppose that only the mass energy or the gap between the two Dirac cones varies from zero to a nonzero value. To achieve a temporal reflectance of 0.05 at a temporal interface, it is necessary to set $f = 0.9$ in Eq. (19), which can be realized by opening a gap of $M = 0.48\hbar k_x v_x$. Similarly, to achieve a maximum temporal reflectance of 0.05 across a temporal slab, it is necessary to set $f^2 = 0.95$ in Eq. (34), which can be accomplished by opening a gap of $M = 0.23\hbar k_x v_x$. These values are relatively small and can be easily achieved using the experimental techniques described in Refs. [41,42].

In conclusion, we have studied the influence of the temporal variations of the medium parameters on the propagation of Dirac-type waves in materials where the quasiparticles are described by a generalized version of the pseudospin-1/2 Dirac equation. We have derived the scattering coefficients associated with the temporal interfaces and slabs analytically and found that the temporal scattering is caused by the changes of the mass, Fermi velocity, and vector potential, but does not arise from the changes of the scalar potential and tilt velocity.

Using the analytical expressions for the temporal transmittances and the interband transition rates, we have obtained the explicit conditions for which the temporal Brewster effect and total interband transition occur. We have also proved that in bilayer Dirac temporal crystals where the parameters alternate between two different values, momentum gaps do not appear in sharp contrast to the classical waves. It is highly desirable to generalize the present investigation to the case where the parameters change arbitrarily in time. This will be a subject of research in the future.

[1] F. R. Morgenthaler, Velocity modulation of electromagnetic waves, IRE Trans. Microwave Theory Tech. **6**, 167 (1958).

[2] L. B. Felsen and G. M. Whitman, Wave propagation in time-varying media, IEEE Trans. Antennas Propag. **18**, 242 (1970).

[3] R. Fante, Transmission of electromagnetic waves into time-varying media, IEEE Trans. Antennas Propag. **19**, 417 (1971).

[4] D. K. Kalluri, *Electromagnetics of Time Varying Complex Media: Frequency and Polarization Transformer*, 2nd ed. (CRC Press, Boca Raton, 2010).

[5] J. T. Mendonça and P. K. Shukla, Time refraction and time reflection: Two basic concepts, Phys. Scr. **65**, 160 (2002).

[6] Y. Xiao, D. N. Maywar, and G. P. Agrawal, Reflection and transmission of electromagnetic waves at a temporal boundary, Opt. Lett. **39**, 574 (2014).

[7] A. G. Hayrapetyan, J. B. Götte, K. K. Grigoryan, S. Fritzsche, and R. G. Petrosyan, Electromagnetic wave propagation in spatially homogeneous yet smoothly time-varying dielectric media, J. Quant. Spectrosc. Radiat. Transfer **178**, 158 (2016).

[8] C. Caloz and Z.-L. Deck-Léger, Spacetime metamaterials—Part I: General concepts, IEEE Trans. Antennas Propag. **68**, 1569 (2020).

[9] C. Caloz and Z.-L. Deck-Léger, Spacetime metamaterials—Part II: Theory and applications, IEEE Trans. Antennas Propag. **68**, 1583 (2020).

[10] D. Ramaccia, A. Toscano, and F. Bilotti, Light propagation through metamaterial temporal slabs: reflection, refraction, and special cases, Opt. Lett. **45**, 5836 (2020).

[11] Y. Zhou, M. Alam, M. Karimi, J. Upham, O. Reshef, C. Liu, A. Willner, and R. Boyd, Broadband frequency translation through time refraction in an epsilon-near-zero material, Nat. Commun. **11**, 2180 (2020).

[12] E. Galiffi, R. Tirole, S. Yin, H. Li, S. Vezzoli, P. A. Huidobro, M. G. Silveirinha, R. Sapienza, A. Alù, and J. B. Pendry, Photonics of time-varying media, Adv. Photon. **4**, 014002 (2022).

[13] R.-Y. Zhang, Y.-W. Zhai, S.-R. Lin, Q. Zhao, W. Wen, and M.-L. Ge, Time circular birefringence in time-dependent magnetoelectric media, Sci. Rep. **5**, 13673 (2015).

[14] X. Wang, G. Ptitcyn, V. S. Asadchy, A. Díaz-Rubio, M. S. Mirmoosa, S. Fan, and S. A. Tretyakov, Nonreciprocity in Bianisotropic Systems with Uniform Time Modulation, Phys. Rev. Lett. **125**, 266102 (2020).

[15] H. Li, S. Yin, and A. Alù, Nonreciprocity and Faraday Rotation at Time Interfaces, Phys. Rev. Lett. **128**, 173901 (2022).

[16] V. Pacheco-Peña and N. Engheta, Temporal aiming, Light Sci. Appl. **9**, 129 (2020).

[17] V. Pacheco-Peña and N. Engheta, Temporal equivalent of the Brewster angle, Phys. Rev. B **104**, 214308 (2021).

[18] F. Biancalana, A. Amann, A. V. Uskov, and E. P. O'Reilly, Dynamics of light propagation in spatiotemporal dielectric structures, Phys. Rev. E **75**, 046607 (2007).

[19] J. R. Zurita-Sánchez, P. Halevi, and J. C. Cervantes-González, Reflection and transmission of a wave incident on a slab with a time-periodic dielectric function $\epsilon(t)$, Phys. Rev. A **79**, 053821 (2009).

[20] T. T. Koutserimpas and R. Fleury, Electromagnetic waves in a time periodic medium with step-varying refractive index, IEEE Trans. Antennas Propag. **66**, 5300 (2018).

[21] E. Lustig, Y. Sharabi, and M. Segev, Topological aspects of photonic time crystals, Optica **5**, 1390 (2018).

[22] E. Galiffi, Y.-T. Wang, Z. Lim, J. B. Pendry, A. Alù, and P. A. Huidobro, Wood Anomalies and Surface-Wave Excitation with a Time Grating, Phys. Rev. Lett. **125**, 127403 (2020).

[23] T. Oka and S. Kitamura, Floquet engineering of quantum materials, Annu. Rev. Condens. Matter Phys. **10**, 387 (2019).

[24] P. Reck, C. Gorini, A. Goussev, V. Krueckl, M. Fink, and K. Richter, Dirac quantum time mirror, Phys. Rev. B **95**, 165421 (2017).

[25] P. Reck, C. Gorini, and K. Richter, Quantum time mirrors for general two-band systems, Phys. Rev. B **98**, 125421 (2018).

[26] V. Junk, P. Reck, C. Gorini, and K. Richter, Floquet oscillations in periodically driven Dirac systems, Phys. Rev. B **101**, 134302 (2020).

[27] A. H. Castro Neto, F. Guinea, N. M. R. Peres, K. S. Novoselov, and A. K. Geim, The electronic properties of graphene, Rev. Mod. Phys. **81**, 109 (2009).

[28] T. Wehling, A. Black-Schaffer, and A. Balatsky, Dirac materials, Adv. Phys. **63**, 1 (2014).

[29] H. Zhang, C.-X. Liu, X.-L. Qi, X. Dai, Z. Fang, and S.-C. Zhang, Topological insulators in $Bi_2 Se_3$, $Bi_2 Te_3$ and $Sb_2 Te_3$ with a single Dirac cone on the surface, Nat. Phys. **5**, 438 (2009).

[30] B. Feng, O. Sugino, R.-Y. Liu, J. Zhang, R. Yukawa, M. Kawamura, T. Iimori, H. Kim, Y. Hasegawa, H. Li, L. Chen, K. Wu, H. Kumigashira, F. Komori, T.-C. Chiang, S. Meng, and I. Matsuda, Dirac Fermions in Borophene, Phys. Rev. Lett. **118**, 096401 (2017).

[31] J. Mei, Y. Wu, C. T. Chan, and Z.-Q. Zhang, First-principles study of Dirac and Dirac-like cones in phononic and photonic crystals, Phys. Rev. B **86**, 035141 (2012).

[32] J. C. Garreau and V. Zehnlé, Simulating Dirac models with ultracold atoms in optical lattices, Phys. Rev. A **96**, 043627 (2017).

[33] M. Milićević, G. Montambaux, T. Ozawa, O. Jamadi, B. Real, I. Sagnes, A. Lemaître, L. Le Gratiet, A. Harouri, J. Bloch, and A. Amo, Type-III and Tilted Dirac Cones Emerging from Flat Bands in Photonic Orbital Graphene, Phys. Rev. X **9**, 031010 (2019).

[34] Y. Li, C. T. Chan, and E. Mazur, Dirac-like cone-based electromagnetic zero-index metamaterials, Light Sci. Appl. **10**, 203 (2021).

[35] M. Li, N. Han, L. Peng, and S. Zhang, Type-II Dirac points and topological Fermi arcs in nonlocal metamaterials, Phys. Rev. B **106**, 235303 (2022).

[36] T. E. O'Brien, M. Diez, and C. W. J. Beenakker, Magnetic Breakdown and Klein Tunneling in a Type-II Weyl Semimetal, Phys. Rev. Lett. **116**, 236401 (2016).

[37] V. H. Nguyen and J.-C. Charlier, Klein tunneling and electron optics in Dirac-Weyl fermion systems with tilted energy dispersion, Phys. Rev. B **97**, 235113 (2018).

[38] S. Kim and K. Kim, Invariant imbedding theory of wave propagation in arbitrarily inhomogeneous stratified bi-isotropic media, J. Opt. **18**, 065605 (2016).

[39] M. Katsnelson, K. Novoselov, and A. Geim, Chiral tunneling and the Klein paradox in graphene, Nat. Phys. **2**, 620 (2006).

[40] J. T. Mendonça, Temporal Klein model for particle-pair creation, Symmetry **13**, 1361 (2021).

[41] Z. Ni, Q. Liu, K. Tang, J. Zheng, J. Zhou, R. Qin, Z. Gao, D. Yu, and J. Lu, Tunable bandgap in silicene and germanene, Nano Lett. **12**, 113 (2012).

[42] S. Ghosal, A. Bandyopadhyay, and D. Jana, Electric field induced band tuning, optical and thermoelectric responses in tetragonal germanene: A theoretical approach, Phys. Chem. Chem. Phys. **22**, 19957 (2020).

[43] A. Díaz-Fernández, L. Chico, J. González, and F. Domínguez-Adame, Tuning the Fermi velocity in Dirac materials with an electric field, Sci. Rep. **7**, 8058 (2017).

[44] T. Farajollahpour, Z. Faraei, and S. A. Jafari, Solid-state platform for space-time engineering: The 8*Pmmn* borophene sheet, Phys. Rev. B **99**, 235150 (2019).

[45] C.-R. Mann, S. Horsley, and E. Mariani, Tunable pseudo-magnetic fields for polaritons in strained metasurfaces, Nat. Photon. **14**, 669 (2020).